

# Locating quantum critical points through singularities of simple observables

Mateusz Łącki<sup>1,2,3</sup>, Bogdan Damski<sup>1</sup>, and Jakub Zakrzewski<sup>1</sup>

<sup>1</sup> *Instytut Fizyki imienia Mariana Smoluchowskiego, Uniwersytet Jagielloński, ulica Łojasiewicza 11, 30-348 Kraków, Poland*

<sup>2</sup> *Institute for Quantum Optics and Quantum Information of the Austrian Academy of Sciences, A-6020 Innsbruck, Austria*

<sup>3</sup> *Institute for Theoretical Physics, University of Innsbruck, A-6020 Innsbruck, Austria*

Quantum critical points are traditionally associated with non-analyticity of the ground state energy reflecting fundamental differences between phases of a system undergoing a quantum phase transition. We discuss how this non-analyticity is passed onto ground state expectation values of different terms of the Hamiltonian. We illustrate our results in the two-dimensional Bose-Hubbard model that can be realized in cold atomic systems. Using quantum Monte Carlo simulations, we show that one can easily extract the position of the critical point in this model from the on-site atom number fluctuations and nearest-neighbor tunnelling. Our results provide a simple experimentally-relevant way of locating critical points in numerous systems undergoing a quantum phase transition.

Standard approaches to finding the critical point in a system undergoing a continuous phase transition are based on the studies of either the excitation spectrum or the correlation functions [1, 2]. The former allows for the identification of the critical point through the expected disappearance of the gap in the excitation spectrum at the critical point. The latter associates the critical point with the divergence of the correlation length providing the characteristic length scale of the asymptotic decay of correlation functions. While these approaches provide significant insights into the nature of the quantum phase transition, they are not necessarily the most practical ways of locating the critical points in real systems.

We describe below a simple way of locating critical points that is complementary to the above approaches and can be actually advantageous in some systems. It is based on the exploration of the defining feature of a quantum phase transition: Non-analyticity of the ground state energy at the quantum critical point (Ch. 1.1 of [1]). While the ground state energy is typically not an observable that can be experimentally measured, it is straightforward to show that the singularity of its derivatives can be easily extracted from simple experimentally-relevant observables.

To justify this statement, we write a generic Hamiltonian describing a system undergoing a quantum phase transition as

$$\hat{H}(\xi) = a(\xi)\hat{H}_1 + b(\xi)\hat{H}_2, \quad (1)$$

where  $\xi$  is the parameter inducing a phase transition such as a magnetic field in spin systems [1, 2] or the intensity of a laser beam in cold atom simulators of Hubbard-like models [3, 4]. We assume that  $\hat{H}_1$  and  $\hat{H}_2$  do not depend on  $\xi$  and that they try to order the system in a different way. This competition leads to the quantum phase transition, whose critical point we denote as  $\xi_c$ .

Next, we write the ground state energy as

$$\mathcal{E} = \langle \xi | \hat{H}_1 | \xi \rangle a + \langle \xi | \hat{H}_2 | \xi \rangle b, \quad (2)$$

where  $|\xi\rangle$  is the ground state wave-function. Using the Feynman-Hellman theorem  $\partial_\xi \mathcal{E} = \langle \xi | \partial_\xi \hat{H} | \xi \rangle$ , where  $\partial_\xi =$

$\partial/\partial\xi$ , we find

$$\partial_\xi \mathcal{E} = \langle \xi | \hat{H}_1 | \xi \rangle \partial_\xi a + \langle \xi | \hat{H}_2 | \xi \rangle \partial_\xi b. \quad (3)$$

Combining Eqs. (2) and (3) we get

$$\langle \xi | \hat{H}_1 | \xi \rangle = \frac{\partial_\xi (\mathcal{E}/b)}{\partial_\xi (a/b)}, \quad \langle \xi | \hat{H}_2 | \xi \rangle = \frac{\partial_\xi (\mathcal{E}/a)}{\partial_\xi (b/a)}. \quad (4)$$

As the quantum critical point is traditionally associated with the non-analyticity of the ground state energy, we assume that the derivatives of the ground state energy with respect to the parameter driving the transition,  $\partial_\xi^m \mathcal{E}(\xi_c)$ , are continuous for  $m = 0, \dots, n-1$  and either divergent or discontinuous at the critical point for  $m = n$ . By differentiating (4) we find that near the critical point

$$\frac{\partial^{n-1}}{\partial \xi^{n-1}} \langle \xi | \hat{H}_1 | \xi \rangle = \frac{1}{b \partial_\xi (a/b)} \frac{\partial^n \mathcal{E}}{\partial \xi^n} + \text{regular at } \xi_c, \quad (5)$$

where the divergent or discontinuous part at the critical point is explicitly separated from the regular part.  $\partial_\xi^{n-1} \langle \xi | \hat{H}_2 | \xi \rangle$  is obtained by exchanging  $a$  and  $b$  in (5).

These equations show how non-analyticity of the ground state energy across the critical point is imprinted onto the  $n-1$  derivative of the ground state expectation value of the different terms of the Hamiltonian. It should be stressed that such a singularity is expected to develop in the limits of temperature  $T \rightarrow 0$  and the system size  $M \rightarrow \infty$ . For finite systems, we expect that instead of a singularity either an extremum or a kink smoothing out discontinuity will develop near the critical point for small enough temperatures.

We will now illustrate how these ideas work in the two-dimensional (2D) Bose-Hubbard model. Such a model can be emulated in a cold atom cloud placed in the optical lattice generated by three standing laser beams producing the periodic potential

$$\xi \cos^2(kx) + \xi \cos^2(ky) + \xi_\perp \cos^2(kz), \quad k = 2\pi/\lambda \quad (6)$$

for atoms (see [3, 5] for a comprehensive discussion of physics of the Bose-Hubbard model and [6–10] for experimental studies of the 2D Bose-Hubbard model). Above

$\lambda$  is the wavelength of the laser beams,  $\xi$  is the height of the optical potential in the  $x$ - $y$  plane where we study the 2D Bose-Hubbard model, and  $\xi_{\perp}$  is the height of the lattice potential confining the atoms to this plane ( $\xi_{\perp} \gg \xi$ ). Additionally, we assume that atoms are kept in an optical lattice by the optical box trap enabling studies of homogeneous systems (see [11, 12] for experiments on cold atoms in box potentials).

It is easy to show using standard techniques that such a system is effectively described by the Hamiltonian [13]

$$\hat{H}(\xi) = -J(\xi) \sum_{\langle \mathbf{i}, \mathbf{j} \rangle} (\hat{a}_{\mathbf{i}}^{\dagger} \hat{a}_{\mathbf{j}} + \hat{a}_{\mathbf{j}}^{\dagger} \hat{a}_{\mathbf{i}}) + \frac{U(\xi)}{2} \sum_{\mathbf{i}} \hat{n}_{\mathbf{i}}(\hat{n}_{\mathbf{i}} - 1),$$

$$[\hat{a}_{\mathbf{i}}, \hat{a}_{\mathbf{j}}^{\dagger}] = \delta_{\mathbf{i}, \mathbf{j}}, [\hat{a}_{\mathbf{i}}, \hat{a}_{\mathbf{j}}] = 0, \hat{n}_{\mathbf{i}} = \hat{a}_{\mathbf{i}}^{\dagger} \hat{a}_{\mathbf{i}}, \quad (7)$$

where  $\langle \mathbf{i}, \mathbf{j} \rangle$  describes nearest-neighbor sites  $\mathbf{i}$  and  $\mathbf{j}$  in the two-dimensional square lattice. Since we assume that  $\xi_{\perp}$  is fixed during the phase transition, the explicit dependence of  $J$  and  $U$  coefficients on  $\xi_{\perp}$  is not displayed.

Comparing this Hamiltonian to (1) and setting  $a(\xi) = -J(\xi)$  and  $b(\xi) = U(\xi)$ , we see that  $\hat{H}_1 = \sum_{\langle \mathbf{i}, \mathbf{j} \rangle} (\hat{a}_{\mathbf{i}}^{\dagger} \hat{a}_{\mathbf{j}} + \hat{a}_{\mathbf{j}}^{\dagger} \hat{a}_{\mathbf{i}})$  describes nearest-neighbor tunnelling between the lattice sites, while  $\hat{H}_2 = \frac{1}{2} \sum_{\mathbf{i}} \hat{n}_{\mathbf{i}}(\hat{n}_{\mathbf{i}} - 1)$  describes on-site atom interactions. Assuming translational invariance of the ground state, which is enforced here by imposing periodic boundary conditions on the system, we obtain  $\langle \xi | \hat{H}_1 | \xi \rangle = 2MC(\xi)$  and  $\langle \xi | \hat{H}_2 | \xi \rangle = M\text{Var}(\xi)/2 + N(N - M)/2M$ , where

$$C(\xi) = \langle \xi | \hat{a}_{\mathbf{i}}^{\dagger} \hat{a}_{\mathbf{j}} + \hat{a}_{\mathbf{j}}^{\dagger} \hat{a}_{\mathbf{i}} | \xi \rangle \Big|_{\langle \mathbf{i}, \mathbf{j} \rangle}$$

is the nearest-neighbor two-point correlation function,

$$\text{Var}(\xi) = \langle \xi | \hat{n}_i^2 | \xi \rangle - \langle \xi | \hat{n}_i | \xi \rangle^2$$

is the variance of on-site atom number operator,  $M$  is the number of lattices sites, and  $N$  is the number of atoms.

The competition between the tunnelling and interactions leads to a quantum phase transition when the average number of atoms per lattice site (the filling factor) is integer [14], which we assume below. The system is in the Mott insulator phase when  $J/U < (J/U)_c$  and it is in the superfluid phase when  $J/U > (J/U)_c$ .

For the unit filling factor being of interest here, the position of the critical point has been discussed in numerous studies and an agreement has been reached that

$$(J/U)_c \approx 0.06. \quad (8)$$

This value was obtained by theoretical studies of the superfluid density [15], compressibility [16], structure factor [17], energy gap [18–21], fixed points of the real-space renormalization group flow [22], and superfluid order parameter [23, 24].

Our approach locates the critical point through the singularities of the derivatives of  $C(\xi)$  and  $\text{Var}(\xi)$ , which

to the best of our knowledge has not been done before. Thus, we propose finding quantum criticality in the two most basic processes captured by the Bose-Hubbard model: Nearest-neighbor tunnelling and on-site atom number fluctuations. Several remarks are in order now.

First, the correlation functions  $\langle \xi | \hat{a}_{\mathbf{i}}^{\dagger} \hat{a}_{\mathbf{j}} + \hat{a}_{\mathbf{j}}^{\dagger} \hat{a}_{\mathbf{i}} | \xi \rangle$  are arguably the most experimentally accessible correlation functions in cold atom systems. It is so because their Fourier transform provides a quasi-momentum distribution of cold atom clouds, which can be extracted from the time-of-flight images [25, 26] (see [6–8] for measurements in the 2D Bose-Hubbard system).

The critical point can be extracted from these correlation functions through the study of their decay with the distance  $|\mathbf{i} - \mathbf{j}|$  between the lattice sites. They are expected to decay exponentially in the Mott phase and algebraically in the superfluid phase in the thermodynamically-large system. Such a strategy of finding the critical point in the 2D Bose-Hubbard model is problematic because the exponential vs. algebraic transition is expected to happen for large  $|\mathbf{i} - \mathbf{j}|$  distances. Such distances are hard to deal with in theoretical calculations because the model is not exactly solvable and it does require substantial computational resources to handle moderate lattices sizes. On the cold atom experimental side, one has to face issues with accurate measurement of distant correlation functions.

Therefore, we would like to argue that our approach provides a more practical way of locating the critical point as it is based on the nearest-neighbor two-point correlation function, which among other correlation functions is the easiest to obtain both theoretically and experimentally.

Second, the variance of the on-site atom occupation can be estimated in-situ thanks to the recent breakthrough in the quantum gas microscopy [27]. This technique allows for the detection of 0, 1, 2, 3 atoms in individual lattice sites. Choosing the sites far away from the borders of the trap, one should be able to minimize the influence of finite-size effects, which should facilitate extraction of the critical point from the experimental data.

Third, the derivatives of the two observables,  $C(\xi)$  and  $\text{Var}(\xi)$ , are proportional to each other [28]

$$\frac{\partial}{\partial \xi} \text{Var}(\xi) = 4 \frac{J(\xi)}{U(\xi)} \frac{\partial}{\partial \xi} C(\xi), \quad (9)$$

so it suffices to measure either one of them.

We perform quantum Monte Carlo (QMC) simulations of the 2D Bose-Hubbard model (7) imposing periodic boundary conditions on the lattice [29, 30]. We divide the Hamiltonian by  $U$ , thereby choosing  $U$  as the unit of energy, and set  $\xi = J/U$  as the parameter driving the transition. Such a popular choice of the parameter driving the transition leads to the same conclusions as the above-discussed possibility of using the height of the

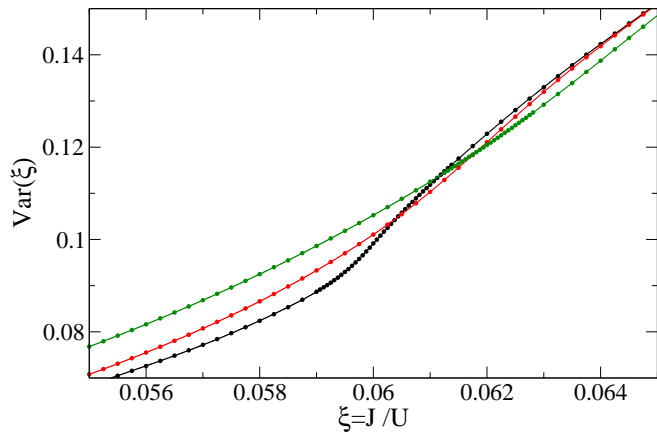


FIG. 1: The variance of the on-site number operator. The circles provide QMC data while the solid lines are Padé approximants (10) fitted to the numerics with parameters  $m \leq 9$  and  $n \leq 6$  (the lower the temperature the higher order polynomials are needed to fit the numerics). The curves from bottom to top (in the left part of the plot) correspond to temperatures  $k_B T/U$  equal to 0.005 (black), 0.04 (red), 0.06 (green), respectively. The system size is  $M = 40^2$ .

optical lattice as  $\xi$ , which requires assuming specific experimental conditions for all numerical simulations.

We compute the variance of the on-site atom occupation for lattice sizes  $M = 10^2$  to  $40^2$  and temperatures  $k_B T/U$  between 0.005 and 0.08. To estimate what such temperatures correspond to, we assume two plausible experimental setups. Namely,  $^{23}\text{Na}$  and  $^{87}\text{Rb}$  atoms placed in the lattice (6) with  $\lambda = 532\text{nm}$  and  $\xi_{\perp} = 30E_R$ , where the recoil energy  $E_R = \hbar^2 k^2 / 2m$  with  $m$  being the mass of the atom. As the s-wave scattering lengths we take 2.8nm for sodium and 5.3nm for rubidium. Computing Wannier functions and proceeding in the standard way [31], we find that the critical point (8) for the sodium (rubidium) system is located at the height of the lattice potential  $\xi_c$  equal to  $10.1E_R$  ( $8.0E_R$ ), for which the coefficient  $U(\xi_c)$  equals  $0.31E_R$  ( $0.51E_R$ ). Having these coefficients, one finds that  $U(\xi_c)/k_B$  equals 461nK for sodium and 199nK for rubidium, respectively. Combining these results, we see that the highest temperatures that we consider are 37nK (16nK) for the above-proposed sodium (rubidium) setup. Both temperatures are experimentally accessible [8–10].

The results that we obtain are presented in Figs. 1–4. To be able to accurately extract the derivatives of the variance, we fit Padé approximants

$$\text{Var}(\xi) = \frac{\sum_{s=0}^m A_s \xi^s}{1 + \sum_{s=1}^n B_s \xi^s}, \quad \xi = \frac{J}{U} \quad (10)$$

to the QMC numerics (Fig. 1) and then differentiate the resulting curves (Figs. 2–4). Such a procedure removes the influence of small fluctuations in the QMC calculations on our results. Moreover, it can be straightfor-

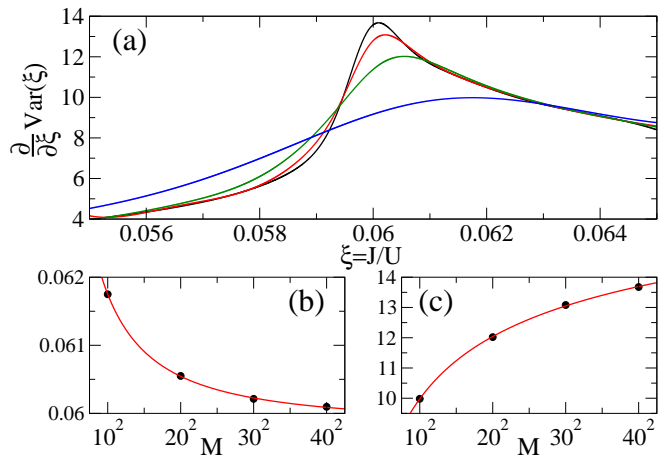


FIG. 2: Plot (a): First derivative of the variance of the on-site number operator. The curves from top to bottom (around the maximum) correspond to  $M$  equal to  $40^2$  (black),  $30^2$  (red),  $20^2$  (green), and  $10^2$  (blue), respectively. Plot (b): The position of the maximum of  $\partial_{\xi}\text{Var}$ . Plot (c):  $\partial_{\xi}\text{Var}$  at the maximum. The circles in plots (b) and (c) show QMC data, while the solid lines provide fits (11) and (12), respectively. All plots are for  $k_B T/U = 0.01$ .

wardly applied to experimental data that will be affected in a similar way by the limited accuracy of measurements.

Looking at Fig. 1, we see that for the lowest temperature displayed,  $k_B T/U = 0.005$ , there is a steep increase of the variance around the critical point (8). Such an abrupt increase is reminiscent of the behavior of magnetization of the 1D quantum Ising model in a transverse field near the critical point [32]. As temperature rises, the abrupt growth of the variance near the critical point fades away and the variance seems to be featureless, which is illustrated for  $k_B T/U = 0.04$  and  $0.06$  in Fig. 1. It is thus worth to stress that the position of the critical point is beautifully imprinted in all the curves from Fig. 1.

In order to extract it, we compute  $\partial_{\xi}\text{Var}$  finding that it has a maximum very close to the critical point (Fig. 2). The position of the maximum,  $\xi_{\max}(M)$ , moves towards the critical point as the system size is increased. To extrapolate it to the thermodynamic limit, we fit

$$\xi_{\max}(M) = a + bM^{-c/2} \quad (11)$$

to QMC data for  $M = 10^2 - 40^2$  and  $k_B T/U = 0.01$  (Fig. 2b; all the fits below are also done for these parameters). We obtain  $a = 0.0598$ ,  $b = 0.0491$ ,  $c = 1.40$ . It turns out that the value of the parameter  $a = \xi_{\max}(\infty)$  is the same as the most accurate estimations of the position of the critical point in the 2D Bose-Hubbard model [16, 20, 21].

Furthermore, we observe that if we fix the system size and vary temperature, then the position of the maximum of  $\partial_{\xi}\text{Var}$  approaches the critical point when  $T \rightarrow 0$  (Fig. 3). Moreover, we observe that  $\partial_{\xi}\text{Var}$  at the maximum grows with both the system size (Fig. 2) and the inverse of the temperature (Fig. 3).

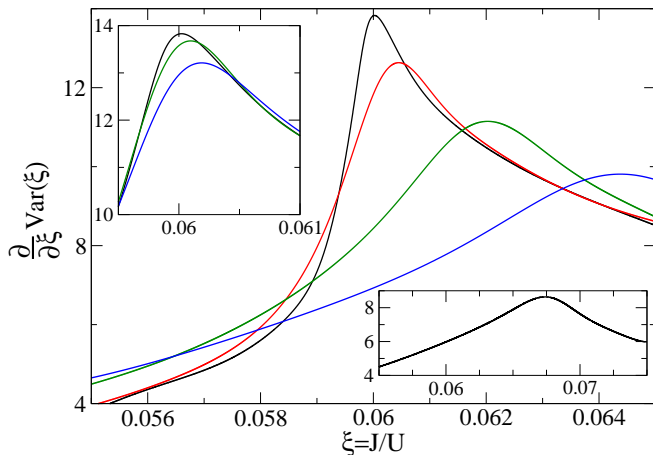


FIG. 3: Derivative of the variance of the on-site number operator. The curves from top to bottom in the main plot correspond to temperatures  $k_B T/U$  equal to 0.005 (black), 0.02 (red), 0.04 (green), 0.06 (blue), respectively. Upper inset illustrates the convergence of our results towards the  $T = 0$  limit. It shows our three lowest-temperature results: from top to bottom  $k_B T/U$  equals 0.005 (black), 0.01 (green), and 0.015 (blue), respectively. Lower inset shows the same as the main plot but for  $k_B T/U = 0.08$ . The system size is  $M = 40^2$  for all the calculations in this figure.

Therefore, it is interesting to ask whether the studied maximum is in fact the singularity that is rounded off and shifted away from the critical point by finite-size effects. To investigate it, we fit  $\partial_\xi \text{Var}(\xi_{\max})$  with

$$\tilde{a} + \tilde{b}M^{\tilde{c}/2}, \quad (12)$$

getting  $\tilde{a} = 20.4$ ,  $\tilde{b} = -21.7$ ,  $\tilde{c} = -0.318$  (Fig. 2c). Taking the limit of  $M \rightarrow \infty$ , we find that instead of a singularity there is a maximum of  $\partial_\xi \text{Var}$  in the thermodynamic limit.

Hunting for a singularity, we compute  $\partial_\xi^2 \text{Var}$  getting the maximum and minimum near the critical point (Fig. 4a). The study of  $\partial_\xi^2 \text{Var}$  at the extrema through the fit (12) supports the conclusion that there is a singularity appearing in the thermodynamic limit (Figs. 4b and 4c). Indeed, for maximum (minimum) we get  $\tilde{a} = -981$ ,  $\tilde{b} = 167$ ,  $\tilde{c} = 1.10$  ( $\tilde{a} = 83.2$ ,  $\tilde{b} = -36.0$ ,  $\tilde{c} = 1.21$ ). This means that as  $M \rightarrow \infty$ , we have  $\partial_\xi^2 \text{Var} \rightarrow \pm\infty$  at the extrema. In-between these extrema there is the point where  $\partial_\xi^2 \text{Var} = 0$ , i.e., where the maximum of  $\partial_\xi \text{Var}$  is located. Thus, in the thermodynamic limit the divergent discontinuity of  $\partial_\xi^2 \text{Var}$  will be located at the same point as the maximum of  $\partial_\xi \text{Var}$  (if that wouldn't be the case, then there would be two points where  $\partial_\xi^2 \text{Var}$  is non-analytic, which would contradict presence of a single critical point in the system). This observation explains why the non-singular in the thermodynamic limit maximum of  $\partial_\xi \text{Var}$  encodes the position of the critical point so accurately.

Finally, we discuss these findings through the scaling theory of phase transitions. The quantum phase tran-

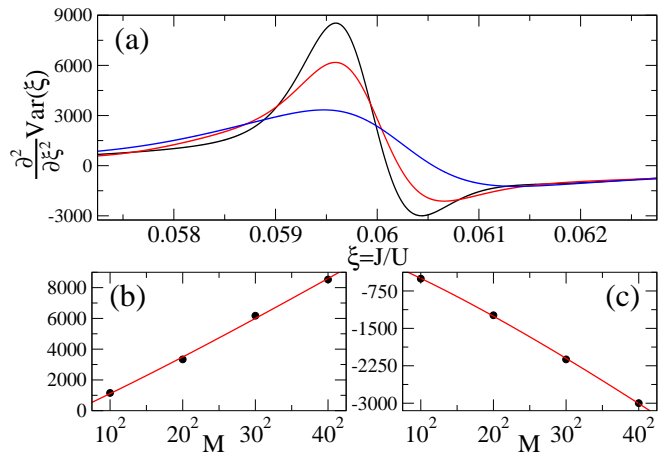


FIG. 4: Plot (a): Second derivative of the variance of the on-site number operator. The curves from top to bottom (around the maximum) correspond to  $M$  equal to  $40^2$  (black),  $30^2$  (red), and  $20^2$  (blue), respectively. Plot (b):  $\partial_\xi^2 \text{Var}$  at the maximum. Plot (c):  $\partial_\xi^2 \text{Var}$  at the minimum. The circles in plots (b) and (c) show QMC data, while the solid lines provide the fit (12). All plots are for  $k_B T/U = 0.01$ .

sition that we study here lies in the universality class of the 3D XY model [14], whose singular part of the free energy scales with the distance  $t$  from the critical point as  $f_s(t) \sim t^{-\alpha}$ , where  $\alpha \approx -0.0146$  [33].  $f_s(t) = f_+(t) - f_-(t)$ , where  $f_+$  ( $f_-$ ) is the free energy for  $t > 0$  ( $t < 0$ ), which has been analytically continued to the complex  $t$  plane [34]. The non-analyticity at the critical point is then seen by non-zero derivative(s) of  $f_s$  at  $t = 0$ . The third and higher derivatives of  $f_s$  are divergent at the critical point of the 3D XY model. Going back from the classical 3D XY model to the quantum 2D Bose-Hubbard model, we expect that the third derivative of the ground state energy will be singular, which translates into the divergent second derivative of the variance through (5). This agrees with our results.

Summarizing, we have proposed that the study of the derivatives of the ground state expectation values of the different terms of the Hamiltonian provides an efficient and experimentally-relevant way of locating quantum critical points. We have illustrated that this is indeed the case in the 2D Bose-Hubbard model that can be realized in cold atom setups. Our results can be immediately applied to other systems undergoing a quantum phase transition such as various spin and strongly correlated electronic systems.

MŁ was supported by Foundation for Polish Science (FNP) and the ERC Synergy Grant UQUAM. BD was supported by the Polish National Science Centre project DEC-2013/09/B/ST3/00239. JZ acknowledges support of EU via project QUIC (H2020-FETPROACT-2014 No. 641122). This research was supported in part by PL-Grid Infrastructure.



- 
- [1] S. Sachdev, *Quantum phase transitions* (Cambridge University Press, Cambridge, 2011).
- [2] S. Sachdev and B. Keimer, *Phys. Today* **64**, 29 (2011).
- [3] M. Lewenstein, A. Sanpera, and V. Ahufinger, *Ultracold Atoms in Optical Lattices: Simulating Quantum Many-Body Systems* (Oxford University Press, Oxford, UK, 2012).
- [4] I. Bloch, J. Dalibard, and S. Nascimbène, *Nature Phys.* **8**, 267 (2012).
- [5] K. V. Krutitsky, *Phys. Rep.* **607**, 1 (2016).
- [6] I. B. Spielman, W. D. Phillips, and J. V. Porto, *Phys. Rev. Lett.* **98**, 080404 (2007).
- [7] I. B. Spielman, W. D. Phillips, and J. V. Porto, *Phys. Rev. Lett.* **100**, 120402 (2008).
- [8] K. Jiménez-García, R. L. Compton, Y.-J. Lin, W. D. Phillips, J. V. Porto, and I. B. Spielman, *Phys. Rev. Lett.* **105**, 110401 (2010).
- [9] W. S. Bakr, A. Peng, M. E. Tai, R. Ma, J. Simon, J. I. Gillen, S. Fölling, L. Pollet, and M. Greiner, *Science* **329**, 547 (2010).
- [10] M. Endres, *Probing correlated quantum many-body systems at the single-particle level* (Springer International Publishing, Switzerland, 2014).
- [11] T. P. Meyrath, F. Schreck, J. L. Hanssen, C.-S. Chuu, and M. G. Raizen, *Phys. Rev. A* **71**, 041604 (2005).
- [12] A. L. Gaunt, T. F. Schmidutz, I. Gotlibovych, R. P. Smith, and Z. Hadzibabic, *Phys. Rev. Lett.* **110**, 200406 (2013).
- [13] D. Jaksch, C. Bruder, J. I. Cirac, C. W. Gardiner, and P. Zoller, *Phys. Rev. Lett.* **81**, 3108 (1998).
- [14] M. P. A. Fisher, P. B. Weichman, G. Grinstein, and D. S. Fisher, *Phys. Rev. B* **40**, 546 (1989).
- [15] W. Krauth and N. Trivedi, *Europhys. Lett.* **14**, 627 (1991).
- [16] J. Šmakov and E. Sørensen, *Phys. Rev. Lett.* **95**, 180603 (2005).
- [17] M. Capello, F. Becca, M. Fabrizio, and S. Sorella, *Phys. Rev. B* **77**, 144517 (2008).
- [18] J. K. Freericks and H. Monien, *Phys. Rev. B* **53**, 2691 (1996).
- [19] L. Amico and V. Penna, *Phys. Rev. Lett.* **80**, 2189 (1998).
- [20] N. Elstner and H. Monien, *Phys. Rev. B* **59**, 12184 (1999).
- [21] B. Capogrosso-Sansone, S. G. Söyler, N. Prokof'ev, and B. Svistunov, *Phys. Rev. A* **77**, 015602 (2008).
- [22] K. G. Singh and D. S. Rokhsar, *Phys. Rev. B* **46**, 3002 (1992).
- [23] N. Teichmann, D. Hinrichs, M. Holthaus, and A. Eckardt, *Phys. Rev. B* **79**, 224515 (2009).
- [24] A. Dutta, C. Trefzger, and K. Sengupta, *Phys. Rev. B* **86**, 085140 (2012).
- [25] M. Greiner, O. Mandel, T. Esslinger, T. W. Hänsch, and I. Bloch, *Nature* **415**, 39 (2002).
- [26] V. A. Kashurnikov, N. V. Prokof'ev, and B. V. Svistunov, *Phys. Rev. A* **66**, 031601 (2002).
- [27] P. M. Preiss, R. Ma, M. E. Tai, J. Simon, and M. Greiner, *Phys. Rev. A* **91**, 041602 (2015).
- [28] B. Damski and J. Zakrzewski, *New J. Phys.* **17**, 125010 (2015).
- [29] A.F. Albuquerque *et al.*, *J. Magn. Magn. Matter.* **310**, 1187 (2007); B. Bauer *et al.*, *J. Stat. Mech.* (2011) P05001.
- [30] We use the Directed Worm Algorithm from the ALPS software package [29]. To evaluate thermodynamical averages, the algorithm samples the space of “worldlines” allowing for the change of the total number of particles. To efficiently evaluate the canonical ensemble averages, the chemical potential is adjusted to yield a unit density in the grand canonical ensemble, thereby maximizing the total number of samples corresponding to the desired average filling factor. In the end, only the “worldlines” with the number of atoms equal to the number of lattice sites are averaged to yield the results presented in Figs. 1–4.
- [31] I. Bloch, J. Dalibard, and W. Zwerger, *Rev. Mod. Phys.* **80**, 885 (2008).
- [32] P. Pfeuty, *Ann. Phys.* **57**, 79 (1970).
- [33] M. Campostrini, M. Hasenbusch, A. Pelissetto, P. Rossi, and E. Vicari, *Phys. Rev. B* **63**, 214503 (2001).
- [34] R. J. Baxter, *Exactly solved models in statistical mechanics* (Academic Press, London, 1982).